

Novel deep learning methods for 3D flow field segmentation and classification

Xiaorui Bai^a, Wenyong Wang^a, Jun Zhang^a, Yueqing Wang^b, Yu Xiang^{a,*}

^aSchool of Computer Science and Engineering, University of Electronic Science and Technology of China, Chengdu, Sichuan, China

^bComputational Aerodynamics Institute, China Aerodynamics Research and Development Center, Mianyang, Sichuan, China

Abstract

Flow field segmentation and classification help researchers to understand vortex structure and thus turbulent flow. Existing deep learning methods mainly based on global information and focused on 2D circumstance. Based on flow field theory, we propose novel flow field segmentation and classification deep learning methods in three-dimensional space. We construct segmentation criterion based on local velocity information and classification criterion based on the relationship between local vorticity and vortex wake, to identify vortex structure in 3D flow field, and further classify the type of vortex wakes accurately and rapidly. Simulation experiment results showed that, compared with existing methods, our segmentation method can identify the vortex area more accurately, while the time consumption is reduced more than 50%; our classification method can reduce the time consumption by more than 90% while maintaining the same classification accuracy level.

Keywords: Three-dimensional space, Deep learning, Flow field segmentation, Flow field classification

1. Introduction

Vortex is a natural phenomenon which plays an important role in aerodynamics, such as turbulent transition, quantum turbulence and energy cascade, etc [1–3]. Vortex is closely related to turbulent flow, a common state of flow and an important area of flow field research. Vortex structures directly affect the generation and evolution of turbulence, and the interaction between vortex structure and turbulence is highly consistent in the wake [4, 5]. Therefore, flow field segmentation and classification to identify and classify vortex structures is essential for turbulence research.

Flow field segmentation, also known as vortex identification, is to identify and extract vortex structures from flow field to study the behaviour of vortices. It is widely applied in aerodynamics, such as accurate prediction of rotor wake and the construction of DNS (direct numerical simulation) boundary layer database, etc [6, 7].

In flow field segmentation area, numerical calculation-based methods and deep learning-based methods are the two most common methods [8].

Methods based on numerical calculation are further divided into local detection methods and global detection methods. Local detection methods such as Q -criterion [9], ω -criterion [10], λ_2 -criterion [11], Δ -criterion [12] and Γ_2 -criterion [13], detected vortex area using local patches and computing new variables. However, local methods rely heavily on the selection of

thresholds to produce valid results, and there are still many false positives and false negatives in the test results. Global methods can obtain high-precision results through global numerical calculations. Sadarjoen extracted vortices using the winding angle and the geometry of streamlines [14]; Serra and Haller created an automated method to efficiently compute closed instantaneous curves using geodesic structures [15]; a threshold-independent method was proposed by Haller to identify vortex based on average vorticity and Instantaneous Vorticity Deviation (IVD) value [16]. The above global detection methods often have an expensive computational time cost due to the complexity of global computation.

Recently, deep learning methods are widely used in this field [17–21]. It is proved to be a compromise way to finish the segmentation task [22], which combines the advantages of local and global methods. Franz and Lguensat tried to use CNN-based binary classification method to identify ocean eddies [23, 24]. Rajendran applied Recurrent Neural Network (RNN) to three-dimensional flow field to locate the eddy current [25]. Wang proposed a fast eddy detection method based on fully convolutional segmentation network [26]. Deng designed a Vortex-U-Net network based on the U-Net model to realize global 3D eddy current detection, which used multiple convolution downsampling for feature extraction and deconvolution upsampling to restore 3D labels [27]. The above-mentioned methods guarantee a certain accuracy rate, but still can be improved in terms of time consumption.

Flow field classification is to classify vortex shedding wake modes in fluid, such as "2S", "2P" and "P+S" mode [28, 29]. It can help understand vortex shedding patterns, which does benefit to vortex shedding suppression and wake control [30]. Besides, flow field classification helps to reduce the unbalanced forces for applications suffering from vortex-induced vibrations

*Corresponding author at: School of Computer Science and Engineering, University of Electronic Science and Technology of China, Chengdu, China.

Email addresses: xrbai@std.uestc.edu.cn (Xiaorui Bai), wangwy@uestc.edu.cn (Wenyong Wang), zhangjun@uestc.edu.cn (Jun Zhang), yqwang2013@163.com (Yueqing Wang), jcxliang@uestc.edu.cn (Yu Xiang)

[31].

In flow field classification area, classification methods can also be simply summarized into two types: classification methods based on local measurements and global information.

Wang and Hemati used the ideal flow method to generate "2S" and "2P" wakes with point vortices, and then used the k-nearest neighbor (KNN) algorithm to classify the wake types [32]. Colvert simulated flow fields with different Strouhal numbers [33], and used the periodicity at fixed points in the flow field as the basis for classification to train the network for flow field classification [34]. Alsaman further investigated how the accuracy of vortex classification is affected by sensor type, and trained a neural network to classify wake types from "one shot" measurement data on a spatially distributed sensor array [35]. Li considered local measurements based on flow variables, and used the flow direction velocity component, transverse velocity component, vorticity and the combination of the three flow variables to train different neural networks to classify the wake structure [36]. Ribeiro explored the kinematics of 46 oscillating wings, combining a convolutional neural network (CNN) with a long short-term memory (LSTM) unit [37]. At the same time, they used the convolutional autoencoder combined with the k-means++ clustering method to verify the physical wake differences between airfoil kinematics, and obtained four different wake patterns. The above methods are mainly based on different oscillation frequencies or global information to classify vortex wakes. However, classification research mainly focuses on 2D cases, and there is a lack of classification for 3D flow fields. Furthermore, processing global information is quite time consuming.

Novel deep learning methods for 3D flow field segmentation and classification based on flow field theory are proposed in this paper. The main contributions of our work are as follows:

(1) The relationship among local vorticity, Reynolds number and vortex wake is explored to construct 3D flow field classification criterion. Then a novel 3D flow field classification deep learning method with high accuracy and low time consumption based on this criterion is proposed.

(2) 3D flow field segmentation criterion identifying vortex through local velocity information is also explored in this paper. A novel flow field segmentation deep learning method, to recognize vortices accurately and rapidly under 3D circumstance, is then proposed.

This paper is organized as follows. Section 2 presents some definitions of flow field and forms the flow field segmentation and classification criteria. Section 3 presents the framework of our flow field segmentation and classification methods. In Section 4, our methods are tested on several classical cases and the corresponding experimental results are analyzed and discussed. Finally, Section 5 concludes our work.

2. Methods

2.1. Problem description and Basic concepts

For segmentation and classification methods we mentioned above, efficiency still needs to be further improved while en-

suring high accuracy. This problem mainly comes from two aspects: criterion and network.

1) *Segmentation criterion and network*: Segmentation criterion determines the selection of data and design of network structure. Obtaining the mapping between velocity data and vortex region is the core issue in constructing segmentation criterion. For segmentation network, increasing network depth for higher accuracy will result in reduced efficiency. To reduce complexity, simple network structure is considered according to segmentation criterion.

2) *Classification criterion and network*: For classification task, an intuitive criterion is to classify flow field based on global information. However, the processing of global information leads to excessive computation, thus reducing classification efficiency. Moreover, existing classification criteria mainly focus on 2D cases. Therefore new 3D classification criterion needs to be constructed. One crucial problem is to obtain the mapping between vorticity data and vortex wake type. And for classification network, global vorticity should be avoided as input, and thus new network also should be considered through classification criterion.

In order to solve the above problems, we start from the following basic concepts.

Given a flow field attribute set $\mathcal{A} = \{\mathbf{p}, t, \mathbf{v}\}$ in 3D flow field \mathcal{F} , each discrete sampling point has its own physical quantities including position $\mathbf{p} = \{x, y, z\}$, time t and velocity $\mathbf{v} = \{u, v, w\}$. With Euler's method, the flow velocity at each position \mathbf{p} within \mathcal{F} could be defined as a function of space position \mathbf{p} and time t . Then, the projections of flow velocity in flow field \mathcal{F} are expressed as follows:

$$\begin{cases} u = u(\mathbf{p}, t) = u(x, y, z, t) \\ v = v(\mathbf{p}, t) = v(x, y, z, t) \\ w = w(\mathbf{p}, t) = w(x, y, z, t) \end{cases}$$

Further, for flow field \mathcal{F} , 3D vorticity is define as the curl of velocity \mathbf{v} and denoted by symbol ω_{3D} [38]. In the Cartesian coordinate system, ω_{3D} is calculated as follows:

$$\begin{aligned} \omega_{3D} = \nabla \times \mathbf{v} &= \omega_x i + \omega_y j + \omega_z k = \begin{vmatrix} i & j & k \\ \frac{\partial}{\partial x} & \frac{\partial}{\partial y} & \frac{\partial}{\partial z} \\ u & v & w \end{vmatrix} \\ &= \left(\frac{\partial w}{\partial y} - \frac{\partial v}{\partial z} \right) i + \left(\frac{\partial u}{\partial z} - \frac{\partial w}{\partial x} \right) j + \left(\frac{\partial v}{\partial x} - \frac{\partial u}{\partial y} \right) k \end{aligned} \quad (1)$$

where ∇ is defined as gradient operator.

2.2. Segmentation criterion

Vorticity has an inseparable relationship with vortex region, but it cannot be directly applied to identify vortices in general [39]. Therefore, it is not feasible to use vorticity to segment the vortex region in our method.

Existing flow field segmentation criteria [9–12] are based on the analysis of the velocity gradient tensor $\nabla \mathbf{v}$ expressed in (2).

$$\nabla \mathbf{v} = \begin{bmatrix} \frac{\partial u}{\partial x} & \frac{\partial u}{\partial y} & \frac{\partial u}{\partial z} \\ \frac{\partial v}{\partial x} & \frac{\partial v}{\partial y} & \frac{\partial v}{\partial z} \\ \frac{\partial w}{\partial x} & \frac{\partial w}{\partial y} & \frac{\partial w}{\partial z} \end{bmatrix} \quad (2)$$

Based on the idea of dividing vorticity into vortical part and non-vortical part [10], velocity gradient tensor ∇v can be rewritten in (3).

$$\nabla v = \frac{1}{2}(\nabla v + \nabla v^T) + \frac{1}{2}(\nabla v - \nabla v^T) = A + B \quad (3)$$

where A is the symmetric part and B is the anti-symmetric part, respectively expressed as follows:

$$A = \frac{1}{2}(\nabla v + \nabla v^T) = \begin{bmatrix} \frac{\partial u}{\partial x} & \frac{1}{2}\left(\frac{\partial u}{\partial y} + \frac{\partial v}{\partial x}\right) & \frac{1}{2}\left(\frac{\partial u}{\partial z} + \frac{\partial w}{\partial x}\right) \\ \frac{1}{2}\left(\frac{\partial v}{\partial x} + \frac{\partial u}{\partial y}\right) & \frac{\partial v}{\partial y} & \frac{1}{2}\left(\frac{\partial v}{\partial z} + \frac{\partial w}{\partial y}\right) \\ \frac{1}{2}\left(\frac{\partial w}{\partial x} + \frac{\partial u}{\partial z}\right) & \frac{1}{2}\left(\frac{\partial w}{\partial y} + \frac{\partial v}{\partial z}\right) & \frac{\partial w}{\partial z} \end{bmatrix}$$

$$B = \frac{1}{2}(\nabla v - \nabla v^T) = \begin{bmatrix} 0 & \frac{1}{2}\left(\frac{\partial u}{\partial y} - \frac{\partial v}{\partial x}\right) & \frac{1}{2}\left(\frac{\partial u}{\partial z} - \frac{\partial w}{\partial x}\right) \\ \frac{1}{2}\left(\frac{\partial v}{\partial x} - \frac{\partial u}{\partial y}\right) & 0 & \frac{1}{2}\left(\frac{\partial v}{\partial z} - \frac{\partial w}{\partial y}\right) \\ \frac{1}{2}\left(\frac{\partial w}{\partial x} - \frac{\partial u}{\partial z}\right) & \frac{1}{2}\left(\frac{\partial w}{\partial y} - \frac{\partial v}{\partial z}\right) & 0 \end{bmatrix}$$

From (3), the first symmetric part is related to deformation while the second anti-symmetric part is related to vorticity [10]. The squares of Frobenius norm of A and B are then introduced as given in (4).

$$a = \text{trace}(A^T A) = \sum_{i=1}^3 \sum_{j=1}^3 (A_{ij})^2 \quad (4)$$

$$b = \text{trace}(B^T B) = \sum_{i=1}^3 \sum_{j=1}^3 (B_{ij})^2$$

Define vector \mathbf{s} in (5) from velocity gradient tensor ∇v in (2).

$$\mathbf{s} = \left[\frac{\partial u}{\partial x}, \frac{\partial u}{\partial y}, \frac{\partial u}{\partial z}, \frac{\partial v}{\partial x}, \frac{\partial v}{\partial y}, \frac{\partial v}{\partial z}, \frac{\partial w}{\partial x}, \frac{\partial w}{\partial y}, \frac{\partial w}{\partial z} \right] \quad (5)$$

Then, a and b can be calculated by \mathbf{s} as shown in (6).

$$a = \mathbf{s} M_1 \mathbf{s}^T \quad b = \mathbf{s} M_2 \mathbf{s}^T \quad (6)$$

where,

$$M_1 = \begin{bmatrix} 1 & 0 & 0 & 0 & 0 & 0 & 0 & 0 & 0 \\ 0 & \frac{1}{4} & 0 & \frac{1}{2} & 0 & 0 & 0 & 0 & 0 \\ 0 & 0 & \frac{1}{4} & 0 & 0 & 0 & \frac{1}{2} & 0 & 0 \\ 0 & 0 & 0 & \frac{1}{4} & 0 & 0 & 0 & 0 & 0 \\ 0 & 0 & 0 & 0 & 1 & 0 & 0 & 0 & 0 \\ 0 & 0 & 0 & 0 & 0 & \frac{1}{4} & 0 & \frac{1}{2} & 0 \\ 0 & 0 & 0 & 0 & 0 & 0 & \frac{1}{4} & 0 & 0 \\ 0 & 0 & 0 & 0 & 0 & 0 & 0 & \frac{1}{4} & 0 \\ 0 & 0 & 0 & 0 & 0 & 0 & 0 & 0 & 1 \end{bmatrix}$$

$$M_2 = \begin{bmatrix} 0 & 0 & 0 & 0 & 0 & 0 & 0 & 0 & 0 \\ 0 & \frac{1}{4} & 0 & -\frac{1}{2} & 0 & 0 & 0 & 0 & 0 \\ 0 & 0 & \frac{1}{4} & 0 & 0 & 0 & -\frac{1}{2} & 0 & 0 \\ 0 & 0 & 0 & \frac{1}{4} & 0 & 0 & 0 & 0 & 0 \\ 0 & 0 & 0 & 0 & 0 & 0 & 0 & 0 & 0 \\ 0 & 0 & 0 & 0 & 0 & \frac{1}{4} & 0 & -\frac{1}{2} & 0 \\ 0 & 0 & 0 & 0 & 0 & 0 & \frac{1}{4} & 0 & 0 \\ 0 & 0 & 0 & 0 & 0 & 0 & 0 & \frac{1}{4} & 0 \\ 0 & 0 & 0 & 0 & 0 & 0 & 0 & 0 & 0 \end{bmatrix}$$

In flow field segmentation methods, scholars usually obtain vortex region by constructing operations related to a and b in (4), such as $(b - a)/2$ or $b/(a + b)$ [9, 10]. Therefore, by the calculation of vector \mathbf{s} in (5), we can get any calculation value of a and b , so as to realize the division of the vortex region.

2.3. Classification criterion

In our research, we construct a novel 3D classification criterion by the following arguments, to overcome the problems in section 2.1.

For flow field \mathcal{F} , the momentum equation is expressed as follows [40]:

$$\nabla \cdot \mathbf{v} = 0$$

$$\frac{\partial \mathbf{v}}{\partial t} + \mathbf{v} \cdot \nabla \mathbf{v} = -\nabla P + \nu \Delta \mathbf{v} \quad (7)$$

where, \mathbf{v} is the velocity field of fluid, t is time, P is pressure field, ∇ is gradient operator, ν is the motion viscosity of fluid.

For (1), by fixing the coordinate component z in the position \mathbf{p} , and setting the velocity component w in the velocity \mathbf{v} to be 0, the process is expressed by (8):

$$\omega_{2D} = \omega_{3D}|_{w=0, z \in [z_0, z_1, \dots, z_n]}$$

$$= \left(\frac{\partial w}{\partial y} - \frac{\partial v}{\partial z} \right) i + \left(\frac{\partial u}{\partial z} - \frac{\partial w}{\partial x} \right) j + \left(\frac{\partial v}{\partial x} - \frac{\partial u}{\partial y} \right) k \Big|_{w=0, z \in [z_0, z_1, \dots, z_n]}$$

$$= \left(\frac{\partial v}{\partial x} - \frac{\partial u}{\partial y} \right) k \quad (8)$$

From (7), we consider the following 9(a) and 9(b) are the components of the 2D incompressible momentum equation [40] in 2D Cartesian coordinate system without external force:

$$\frac{\partial u}{\partial t} + u \frac{\partial u}{\partial x} + v \frac{\partial u}{\partial y} = -\frac{1}{\rho} \frac{\partial P}{\partial x} + \nu \left(\frac{\partial^2 u}{\partial x^2} + \frac{\partial^2 u}{\partial y^2} \right) \quad (a)$$

$$\frac{\partial v}{\partial t} + u \frac{\partial v}{\partial x} + v \frac{\partial v}{\partial y} = -\frac{1}{\rho} \frac{\partial P}{\partial y} + \nu \left(\frac{\partial^2 v}{\partial x^2} + \frac{\partial^2 v}{\partial y^2} \right) \quad (b) \quad (9)$$

It is common to solve the dimensionless basic equations of fluid mechanics [41]. Define the dimensionless parameters as follows:

$$\hat{x} = \frac{x}{L} \quad \hat{y} = \frac{y}{L} \quad \hat{u} = \frac{u}{U} \quad \hat{v} = \frac{v}{U} \quad \hat{P} = \frac{P}{\rho U^2} \quad \hat{t} = \frac{U t}{L}$$

where L is the characteristic length (usually the diameter of the pipeline), U represents the feature speed, and the ρ is the flow field density.

Thus, (9) can be converted into the following dimensionless form:

$$\frac{\partial \hat{u}}{\partial \hat{t}} + \hat{u} \frac{\partial \hat{u}}{\partial \hat{x}} + \hat{v} \frac{\partial \hat{u}}{\partial \hat{y}} = -\frac{\partial \hat{P}}{\partial \hat{x}} + \frac{1}{Re} \left(\frac{\partial^2 \hat{u}}{\partial \hat{x}^2} + \frac{\partial^2 \hat{u}}{\partial \hat{y}^2} \right) \quad (a)$$

$$\frac{\partial \hat{v}}{\partial \hat{t}} + \hat{u} \frac{\partial \hat{v}}{\partial \hat{x}} + \hat{v} \frac{\partial \hat{v}}{\partial \hat{y}} = -\frac{\partial \hat{P}}{\partial \hat{y}} + \frac{1}{Re} \left(\frac{\partial^2 \hat{v}}{\partial \hat{x}^2} + \frac{\partial^2 \hat{v}}{\partial \hat{y}^2} \right) \quad (b) \quad (10)$$

where $Re = UL/\nu$. Reynolds number (Re) is a dimensionless quantity that helps predict fluid flow patterns in different situations.

Through the following calculation:

$$\frac{\partial}{\partial \hat{x}} [Eq. 5(b)] - \frac{\partial}{\partial \hat{y}} [Eq. 5(a)]$$

The dimensionless vorticity transport equation can be obtained in (11).

$$\frac{\partial \omega_{2D}}{\partial \hat{t}} = \frac{1}{Re} \left(\frac{\partial^2 \omega_{2D}}{\partial \hat{x}^2} + \frac{\partial^2 \omega_{2D}}{\partial \hat{y}^2} \right) - \left(\hat{u} \frac{\partial \omega_{2D}}{\partial \hat{x}} + \hat{v} \frac{\partial \omega_{2D}}{\partial \hat{y}} \right) \quad (11)$$

Then, (11) could be expanded in 3D form as follows:

$$\begin{aligned} \left. \frac{\partial \omega_{3D}}{\partial \hat{t}} \right|_{w=0} &= \bigcup_{z=[z_0, z_1, \dots, z_n]} \left. \frac{\partial \omega_{3D}}{\partial \hat{t}} \right|_{w=0} \\ &= \left(\frac{1}{Re} \left(\frac{\partial^2 \omega_{3D}}{\partial \hat{x}^2} + \frac{\partial^2 \omega_{3D}}{\partial \hat{y}^2} \right) - \left(\hat{u} \frac{\partial \omega_{3D}}{\partial \hat{x}} + \hat{v} \frac{\partial \omega_{3D}}{\partial \hat{y}} \right) \right) \bigg|_{w=0, z=z_0, z_1, \dots, z_n} \end{aligned} \quad (12)$$

The derivation of classification criterion then can be divided into two steps:

1) The relationship between $\partial \omega / \partial t$ and Re .

We start from 2D case. In our research, we fix arbitrary point (x, y) in 2D flow field. Referring to (11), $\hat{u} (\partial \omega / \partial \hat{x}) + \hat{v} (\partial \omega / \partial \hat{y})$ is the convection term which describes the motion of the fluid particle as it moves from one point (x_0, y_0) to another (x_1, y_1) . $\partial^2 \omega / \partial \hat{x}^2 + \partial^2 \omega / \partial \hat{y}^2$ term is the diffusion term. Then Equation (11) represents that $\partial \omega / \partial t$ is controlled by the convection term, the diffusion term and Reynolds number. In our research, we only consider the vorticity change in time dimension, and thus regard the diffusion term and convection term at a fixed point (x, y) as constants. Then we get the following (13) from (11):

$$\frac{\partial \omega_{2D}}{\partial \hat{t}} \propto \left(\frac{m}{Re} + n \right) \quad (13)$$

where m represents the diffusion term, n represents the convection term, m and n are constants, and $\partial \omega_{2D} / \partial \hat{t}$ represents 2D vorticity change rate with time.

In 3D case, we get the following (14) from (12):

$$\left. \frac{\partial \omega_{3D}}{\partial \hat{t}} \right|_{w=0} \propto \left(\frac{m}{Re} + n \right) \bigg|_{w=0, z=z_0, z_1, \dots, z_n} \quad (14)$$

2) The relationship between Re and vortex wake.

Williamson and Roshko [28] performed experimental studies of different vortex shedding modes on oscillating cylinders with Reynolds numbers from 300 to 1000. They found that when $Re < 300$, the whole region is dominated by P+S mode, and when $300 < Re < 1000$, the flow field will change from P+S mode to 2P mode at a certain boundary. In Han's work [42], as the Reynolds number changes, the main shedding mode of vortex also changes. Previous researches showed that vortex mode could be determined by Reynolds number under specific conditions.

Above analysis shows that $\partial \omega_{2D} / \partial t$ can be employed to differentiate 3D flow fields with different Reynolds numbers and further to classify the types of vortex wakes in 3D flow field.

3. Methods framework

Three problems must be solved in the framework of our methods: 1) generating input data from above segmentation criterion; 2) generating input data according to the mapping between vorticity and vortex wake type from above classification criterion; 3) establishing segmentation and classification networks. The general framework of our methods to solve these three problems are presented below.

The methods framework, as shown in Fig. 1, consists of three modules: preprocessing module, flow field segmentation module and flow field classification module. Preprocessing module is to process the continuous data into discrete form and generate data for flow field segmentation and classification modules. Subsequently, flow field segmentation module trains the network to judge the vortex region and perform visualization operations. Finally, flow field classification module classifies flow fields with different Reynolds numbers and map them to corresponding vortex types.

3.1. Preprocessing module

The flow field data is provided in form of network common data form (netCDF) [43], which contains flow velocity values in each direction of each time step and 3D grid points, so that the data points obtained by sampling are discrete point sets in continuous flow field space. For discrete dataset, we need to redefine the discrete point set and the corresponding velocity and coordinate components of the sampling point. Therefore, define $\mathcal{F}_d = \{p_{i,j,k}^t, i = 0, \dots, I, j = 0, \dots, J, k = 0, \dots, K\}$ as the grid point set of 3D flow field \mathcal{F} at time t in 3D Cartesian coordinate system, $t = \{0, 1, \dots, T\}$. Define the components of the coordinate data at the point $p_{i,j,k}^t$ in each direction of the 3D Cartesian coordinate system to be x_i, y_j, z_k respectively, and the components of the flow velocity vector in each direction are $u_{i,j,k}^t, v_{i,j,k}^t, w_{i,j,k}^t$.

The vorticity calculation at discrete coordinate points adopts finite difference method (FDM) [44] for spatial discretization, and the central difference form of components in each direction of 3D vorticity at point $p_{i,j,k}^t$ is expressed as follows:

$$\begin{aligned} \frac{\partial w}{\partial y} - \frac{\partial v}{\partial z} &= \frac{w_{i+1,j,k}^t - w_{i-1,j,k}^t}{y_{i+1} - y_{i-1}} - \frac{v_{i,j+1,k}^t - v_{i,j-1,k}^t}{z_{j+1} - z_{j-1}} \\ \frac{\partial u}{\partial z} - \frac{\partial w}{\partial x} &= \frac{u_{i+1,j,k}^t - u_{i-1,j,k}^t}{z_{i+1} - z_{i-1}} - \frac{w_{i,j+1,k}^t - w_{i,j-1,k}^t}{x_{j+1} - x_{j-1}} \\ \frac{\partial v}{\partial x} - \frac{\partial u}{\partial y} &= \frac{v_{i+1,j,k}^t - v_{i-1,j,k}^t}{x_{i+1} - x_{i-1}} - \frac{u_{i,j+1,k}^t - u_{i,j-1,k}^t}{y_{j+1} - y_{j-1}} \end{aligned} \quad (15)$$

3.1.1. Input data generation for segmentation

As described in section 2.2, the items in vector \mathbf{s} in (5) are selected as the input in our method. This allows us to map vector \mathbf{s} to two-dimensional vector (vortex and non-vortex), which can be achieved using Multi-layer Perception (MLP).

Through FDM, we fit vector \mathbf{s} in each discrete point x_i, y_j, z_k by selecting data from u, v and w according to (15). Therefore,

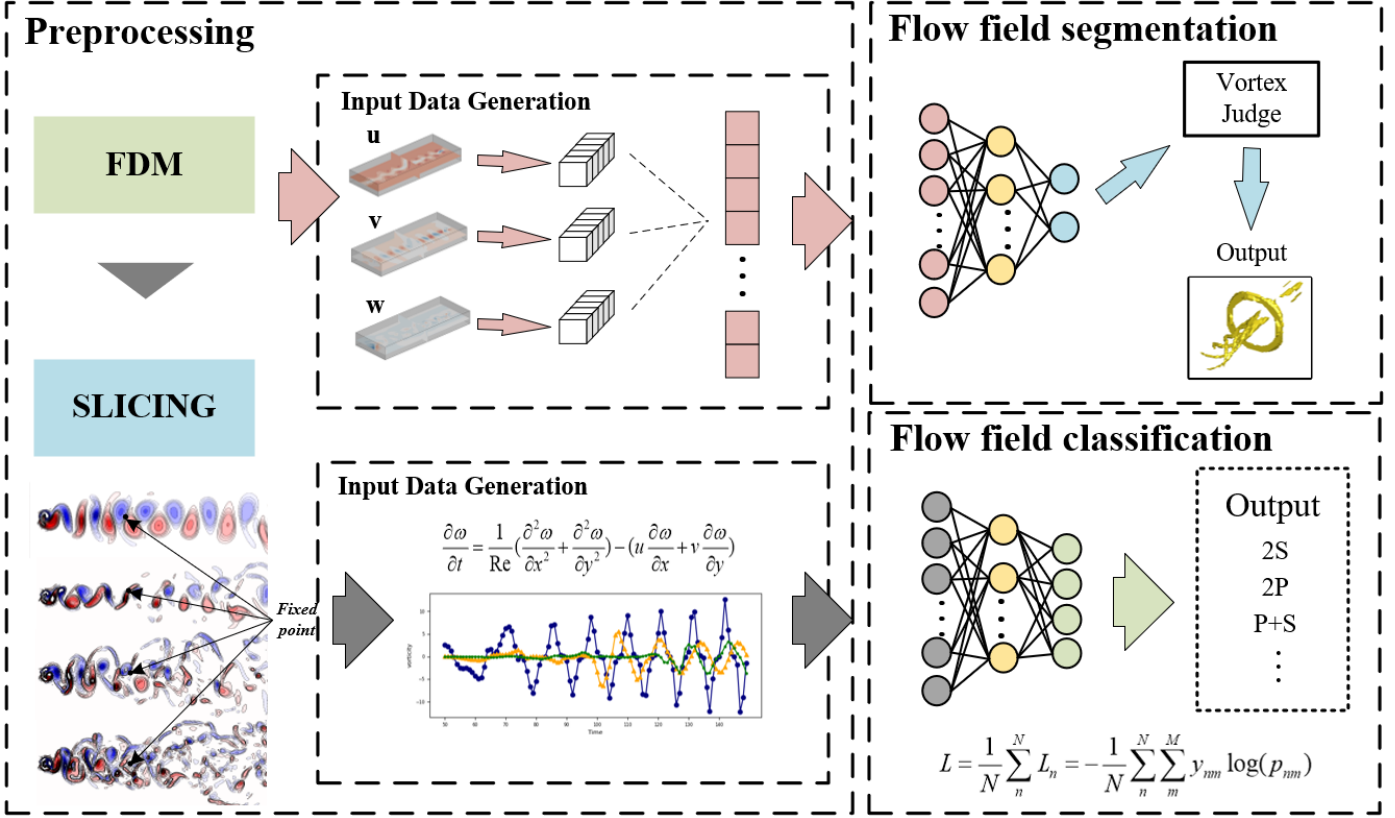


Figure 1: The framework of flow field segmentation and classification methods.

our research selects the 15-dimensional vector $\mathbf{s}_{i,j,k}$ in x_i, y_j, z_k , as the input as follows:

$$\begin{aligned}
 \mathbf{u}_{i,j,k} &= [u_{i,j-1,k}^t, u_{i,j,k}^t, u_{i,j+1,k}^t, u_{i,j,k-1}^t, u_{i,j,k+1}^t] \\
 \mathbf{v}_{i,j,k} &= [v_{i-1,j,k}^t, v_{i,j,k}^t, v_{i+1,j,k}^t, v_{i,j,k-1}^t, v_{i,j,k+1}^t] \\
 \mathbf{w}_{i,j,k} &= [w_{i-1,j,k}^t, w_{i,j,k}^t, w_{i+1,j,k}^t, w_{i,j-1,k}^t, w_{i,j+1,k}^t] \\
 \mathbf{s}_{i,j,k} &= \mathbf{u}_{i,j,k} \cup \mathbf{v}_{i,j,k} \cup \mathbf{w}_{i,j,k}
 \end{aligned} \quad (16)$$

3.1.2. Input data generation for classification

Referring to ω_{2D} described in (8) and difference form described in (15), the sliced 3D vorticity value ω_{2D} is obtained.

At a fixed point, $\partial\omega_{2D}/\partial t$ can be learned by learning the periodicity of vorticity through neural network. And by classifying $\partial\omega_{2D}/\partial t$ can realize the classification of 3D flow fields with different Reynolds numbers.

Therefore, ω_{2D} at each sampling time t is selected as the input data. According to FDM, the differential form of $\partial\omega_{2D}/\partial t$:

$$\frac{\partial\omega_{2D}}{\partial t} = \frac{\omega_{i,j,k}^{t+1} - \omega_{i,j,k}^{t-1}}{2\Delta t}$$

Simultaneously, fixing $j = (J+1)/2$ (select the points where vorticity changes significantly), our research generates the input vector of neural network in (17).

$$\mathbf{s}_{i,k} = [\omega_{i,j,k}^0, \omega_{i,j,k}^1, \dots, \omega_{i,j,k}^T], \quad j = (J+1)/2 \quad (17)$$

According to the above input vector $\mathbf{s}_{i,k}$, deep learning method can learn $\partial\omega_{2D}/\partial t$ at any time t .

3.2. Flow field segmentation module

The local flow velocity information $\mathbf{s}_{i,j,k}$ of each point is obtained through (16) and input into the corresponding flow field segmentation network respectively. In 3D case, our network is expressed as

$$\begin{cases}
 y_n = f_{MLP_seg}(S_{i,j,k}, \theta_{seg}) \\
 i = 1, \dots, I, \quad j = 1, \dots, J, \quad k = 1, \dots, K \\
 \theta_{seg} = \{W, b\} \sim U\left(-\sqrt{\frac{3}{l}}, \sqrt{\frac{3}{l}}\right), U\left(-\sqrt{\frac{1}{l}}, \sqrt{\frac{1}{l}}\right)
 \end{cases}$$

where θ_{seg} is the initialization parameter set, W and b are the weight and bias of our network, and l is the amount of input data of each linear layer.

According to network structure, this network uses the *Relu* function as the activation function. To deal with segmentation problem, the binary cross-entropy loss function is used to train our network, as follows:

$$Loss(\hat{y}_n, y_n) = \frac{1}{N} \sum_n -[y_n \log(\hat{y}_n) + (1 - y_n) \log(1 - \hat{y}_n)] \quad (18)$$

where N represents the number of samples, n represents the sample sequence, y_n represents the predicted value of the n^{th} sample, and \hat{y}_n represents the true value of the n^{th} sample.

Table 1
Summary of training and testing flow field datasets

	Type	Case	Name	Grid Size	No.	Exp
Flow field segmentation	2D	Cylinder	cylinder2d	640 × 80	1	I
	3D	ShockWave	SV81-1000	81 × 81 × 81	2.1	II.(1), II.(2)
			SV81-1500	81 × 81 × 81	2.2	
			SV161-2000	161 × 81 × 81	2.3	
	Turbulence	turbulence	65 × 65 × 65	3	III	
Flow field classification	3D	Half-Cylinder	half-cylinder160	640 × 240 × 80	4.1	IV.(1), IV.(2)
			half-cylinder320	640 × 240 × 80	4.2	
			half-cylinder640	640 × 240 × 80	4.3	
			half-cylinder6400	640 × 240 × 80	4.4	

3.3. Flow field classification module

After preprocessing the local calculation of vorticity in (17), vector $\mathbf{s}_{i,k}$ is input into multi-layer perceptron for learning,

$$\begin{cases} y_n = f_{MLP,clas}(\mathbf{s}_{i,k}, \theta_{clas}) \\ i = 1, \dots, I, k = 1, \dots, K \\ \theta_{clas} = \{W, b\} \sim U\left(-\sqrt{\frac{3}{l}}, \sqrt{\frac{3}{l}}\right), U\left(-\sqrt{\frac{1}{l}}, \sqrt{\frac{1}{l}}\right) \end{cases}$$

where y_n is the output value obtained from the n^{th} selected point in 3D flow field, θ_{clas} is the initialization parameter set, W and b are the weight and bias of this model, and l is the amount of input data of each linear layer.

The multi-classification cross-entropy loss function is used to train our model. Besides, the Adam optimizer is used to iteratively update the network parameters. The form of our loss function is expressed as follow:

$$Loss(\hat{y}_n, y_n) = \frac{1}{N} \sum_n L_n(\hat{y}_n, y_n) = -\frac{1}{N} \sum_n \sum_m y_{nm} \log(p_{nm}) \quad (19)$$

where N represents the number of samples, M represents the number of categories, n represents the sample sequence, m represents the vector number, y_n represents the predicted value of the n^{th} sample, and \hat{y}_n represents the true value of the n^{th} sample. y_{nm} is a sign function (0 or 1), and if the category m of the sample n is the real category, the sign function takes 1, otherwise it takes 0. p_{nm} is the predicted probability that the observed sample belongs to category m .

4. Results and discussions

4.1. Data and Experimental Setup

This section introduces the datasets required for experiment and its related parameters. Then, prepare several sets of experiments separately for flow field segmentation and classification.

4.1.1. Datasets

To verify the performance of our flow field segmentation and classification method, we utilize several 2D and 3D cases as task datasets.

In segmentation task, cases are selected as follows:

Cylinder [45]: This public dataset is derived from the simulation of a viscous 2D flow around a cylinder using the Gerris flow solver [46]. The regular grid resolution is 640 × 80 and the Reynolds number is 160.

Shockwave (SV): This 3D datasets consists of three data sets: SV81-1000, SV81-1500 and SV161-2000. The grid resolution of SV81-1000 and SV81-1500 are 81 × 81 × 81 with their Reynolds numbers are 1000 and 1500 respectively. The grid resolution of SV161-2000 is 161 × 81 × 81 with Reynolds numbers is 2000.

Turbulence: This 3D dataset is derived from the simulation of a viscous 3D flow and the regular grid resolution is 65 × 65 × 65.

In classification task, cases are selected as follows:

Half Cylinder [47]: This public dataset is a small collection of simulated incompressible 3D flows around a half cylinder generated using the Gerris flow solver [46], where the Reynolds number ranges from 160 to 6400 (Re: 160, 320, 640, and 6400). The regular grid resolution is 640 × 240 × 80, and the data is provided in the network common data table (netCDF) format [43]. The 3D isosurface diagram of this flow field at a Reynolds number of 160 is shown in Fig. 2.

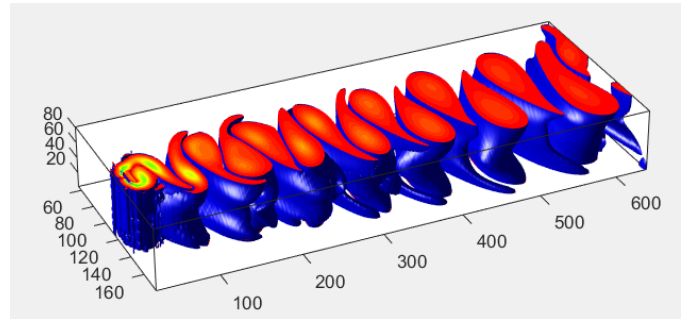


Figure 2: 3D isosurface map of Half Cylinder dataset when Re = 160

In Table 1, we summarize the dataset information of the flow field segmentation and flow field classification experiments, and their related parameters.

4.1.2. Experimental Setup

As shown in Table 1, we set up the following sets of experiments based on the above datasets.

In segmentation task:

Cylinder: In Exp I, this experiment randomly divide sampling points in dataset 1 by 8:2 and obtain 40,960 training data and 10,240 test data.

Shockwave (SV): In the case of shockwave, two different experiments are performed to validate our method. In Exp II.(1), dataset 2.1 with a size of $81 \times 81 \times 81$ is used as the training set and Dataset 2.2 with a size of $81 \times 81 \times 81$ is used as the testing set. In Exp II.(2), after randomly dividing dataset 2.1 and dataset 2.3 by 8:2, these two dataset are combined in a ratio of 8:2 to obtain training set and test set.

Turbulence: In Exp III, this experiment randomly divide sampling points in dataset 3 by 8:2 and obtain 219,700 training data and 54,925 test data.

In flow field classification experiment, as shown in Table 1, we set up the following sets of experiments.

Half Cylinder: In Exp IV.(1) and Exp IV.(2), we select datasets 4.1, 4.2 and datasets 4.1, 4.2, 4.3, 4.4 respectively.

Through dimensionality reduction, 80 2D flow field cutting planes can be selected from each 3D dataset. In each cut plane, 640 input vectors can be obtained through data selection. For cross-validation, we divide each 3D dataset into 5 groups with each group has 16 2D cut plane. For each group, 80% of the data is selected for training, and the remaining 20% is selected for testing. That is, 5 groups of experiments can be carried out in Exp IV.(1) and Exp IV.(2).

4.2. Benchmark methods and Metrics

In flow field segmentation experiments, our method is compared with four other techniques, which are defined as follows:

Vortex-Net [48]: a segmentation CNN to detect vortices from the velocity field.

Vortex-Seg-Net [26]: a fully convolutional method for flow field segmentation.

U-Net: 3D eddy detection method based on U-Net.

IVD [16]: a threshold-independent vortex detection technique based on the outermost closed-level sets of the IVD value.

In flow field classification experiments, our method is compared with three common image processing methods, which are defined as follows:

CNN [37]: a common convolutional method suitable for image classification.

FCN: a fully convolutional method modified for classification task.

U-Net: a classification network based on U-Net modified for classification task.

The performances for segmentation and classification methods are measured by precision, recall, accuracy and time consumption. Precision and recall rate are as shown below:

$$Precision = \frac{TP}{TP + FP}$$

$$Recall = \frac{TP}{TP + FN}$$

Table 2

Hyperparameters for the flow field segmentation experiments

Type	MLP Exp I	MLP Exp II.(1)	MLP Exp II.(2)	MLP Exp III
Input	6	15	15	15
Hidden layer1	128	64	64	64
Hidden layer2	128	64	64	64
Output	2	2	2	2
Learning rate	0.005	0.005	0.005	0.005
Epoch	500	500	500	500
Batch size(Training)	128	19,683	39,123	4,225
Batch size(Testing)	1,024	19,683	19,683	4,225

where TP , FP , TN , and FN mean the number of true positives, false positives, true negatives, and false negatives.

4.3. Experimental results

4.3.1. Results for flow field segmentation

The hyper-parameters for flow field segmentation experiment are summarized in Table 2.

Each indicator is the average calculation result obtained after repeated training 10 times under different random seeds. Table 4 presents the accuracy and time-consuming performance of all mainstreaming methods in flow field segmentation experiments.

Table 3

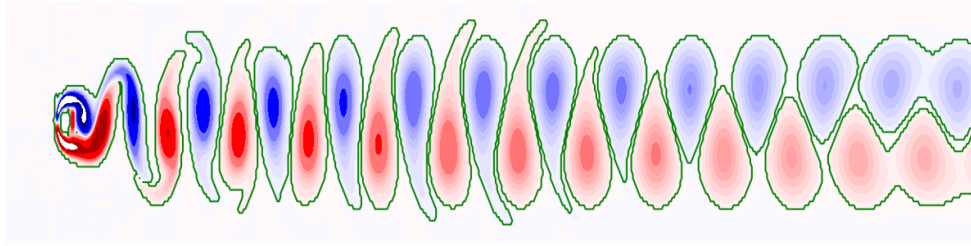
Experiment results for flow field segmentation

Experiment	Method	Precision	Recall	Time Consumption (s)
Exp I	MLP	99.30%	98.87%	2.3
	IVD	100%	100%	432
Exp II.(1)	Vortex-Net	76.68%	89.25%	565
	Vortex-Seg-Net	82.26%	81.16%	43.2
	U-Net	86.17%	84.25%	22.3
	MLP	90.76%	82.73%	4.5
Exp II.(2)	IVD	100%	100%	3023
	MLP	90.77%	84.30%	6.1
Exp III	IVD	100%	100%	4435
	Vortex-Net	85.22%	95.23%	76.2
	Vortex-Seg-Net	92.23%	97.06%	20.1
	U-Net	97.86%	98.14%	12.1
	MLP	98.87%	97.92%	4.7
	IVD	100%	100%	3879

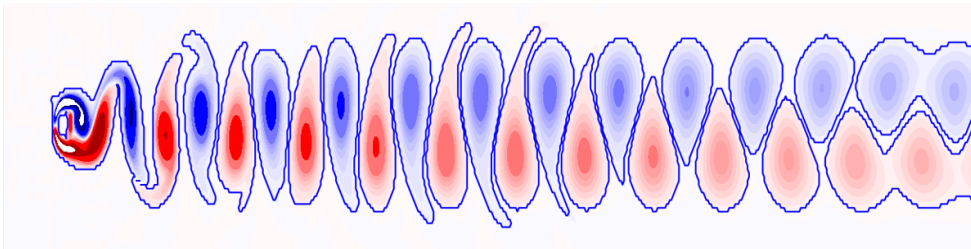
Cylinder: In Exp I, compared with the label area, its accuracy rate is as high as 99.40%. At the same time, the precision and recall rate under this experiment respectively reaches 99.30% and 98.87%.

Experimental results verify the applicability of our method for flow field segmentation in the case of 2D cylinder.

Shockwave: In Exp II.(1) and Exp II.(2), the experiments respectively achieve 99.75% and 99.77% accuracy. From Table 3,



(a) Vortex zone labeled by IVD method



(b) Flow field segmentation result

Figure 3: The visual results in Exp I on Cylinder case.



(a) Vortex-Net method



(b) Vortex-Seg-Net method



(c) U-Net method



(d) MLP method

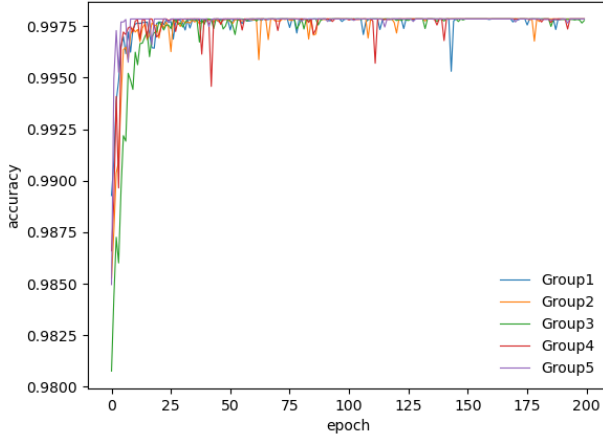


(e) IVD method

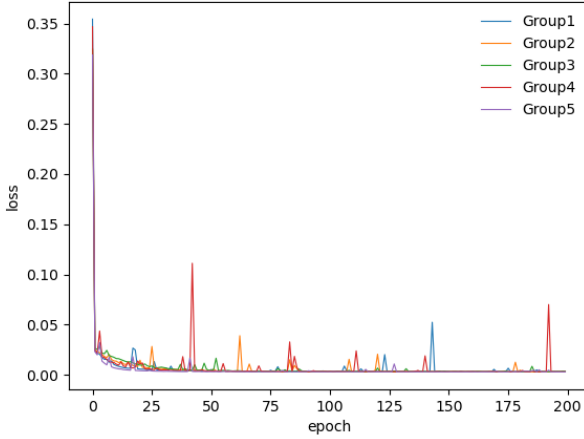
Figure 4: The visual results of different methods in Exp II.(1) on ShockWave case.

compared with the best result (U-Net) in the baseline methods, the precision of our method is 4% higher in Exp II.(1). In terms of recall rate, the results of Exp II.(1) show that our method has a small decrease of 1.5% and 6% compared with U-Net method

and CNN method. In terms of time consumption, the time of our method is 18 seconds less than that of the U-Net method, and it is also much shorter than label method. In Exp II.(2), other methods cannot be used as comparative experiments due



(a) test accuracy



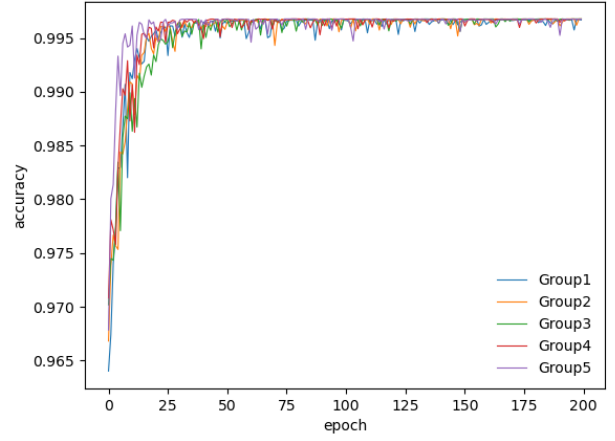
(b) test loss

Figure 5: The training loss and test loss and accuracy curve of our method in Exp IV.(1).

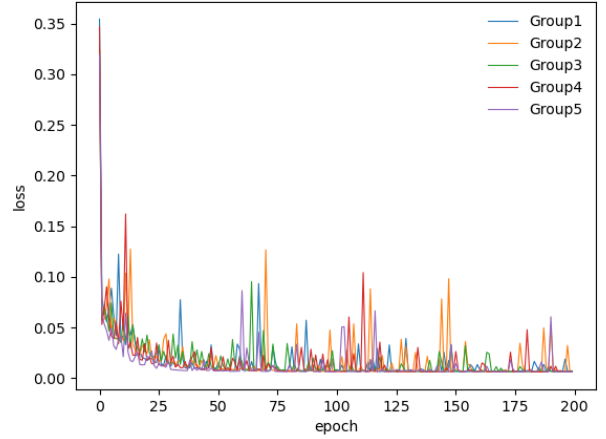
to the experimental setup. Our method achieved a precision of 90.77% and a recall rate of 84.30% in Exp II.(2). What's more, the consumption time of our method is much lower than IVD method.

Turbulence: In Exp III, the turbulence case is tested by multiple methods. Compared with the U-Net method, our method is 1% higher in accuracy. In terms of time consumption, this method is improved by 8 seconds compared with the U-Net method.

In the above comparison experiments, our method greatly reduces time consumption in Exp II.(1) and Exp III compared with the best benchmark method (U-Net). To shockwave case and turbulence case, the precision of our method is higher than that of U-Net method while ensuring low time consumption. In conclusion, compared with traditional numerical calculation methods, such as IVD, our method can complete the segmentation task in a short time while ensuring high accuracy. Com-



(a) test accuracy



(b) test loss

Figure 6: The training loss and test loss and accuracy curve of our method in Exp IV.(2).

pared with deep learning-based methods such as U-Net, our method has a simpler structure and more efficient segmentation capabilities, so the verification of our method takes less time. Simultaneously, our method is a single-point judgment method based on local information, and its judgment accuracy in ShockWave case and turbulence case is also higher than that of methods based on global information.

Then use tecplot to draw the detection results to observe the vortex region more intuitively.

In Exp I, the vortex division of 2D cylinder flow field is shown in Fig. 3. In Fig. 3(a), the global detection method IVD [16] demarcates the labeled vortex region. Fig. 3(b) shows the vortex area divided by our method. In addition, the center area of the vortex around the cylinder is perfectly divided, and the wrong part is only the edge of the vortex.

In Exp II.(1), the visualization results of all methods in SV case are shown in Fig. 4. Although in Fig. 4(d), there are some

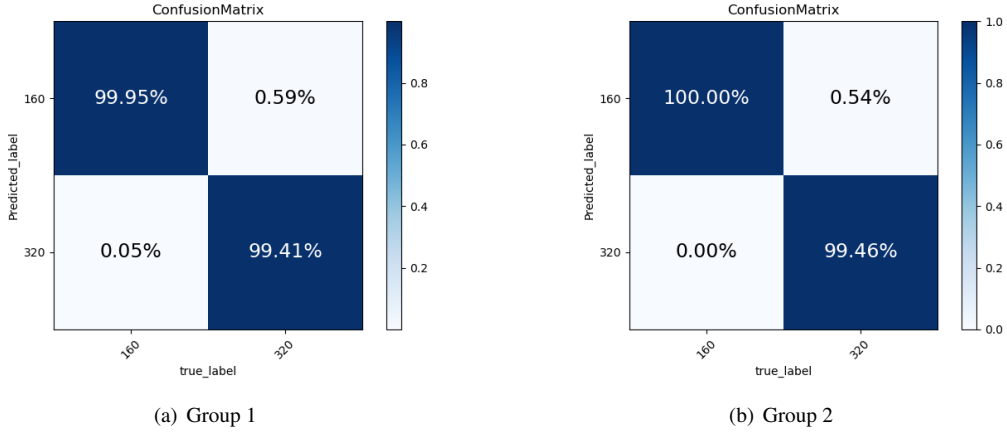


Figure 7: Confusion matrixes in Exp IV.(1).

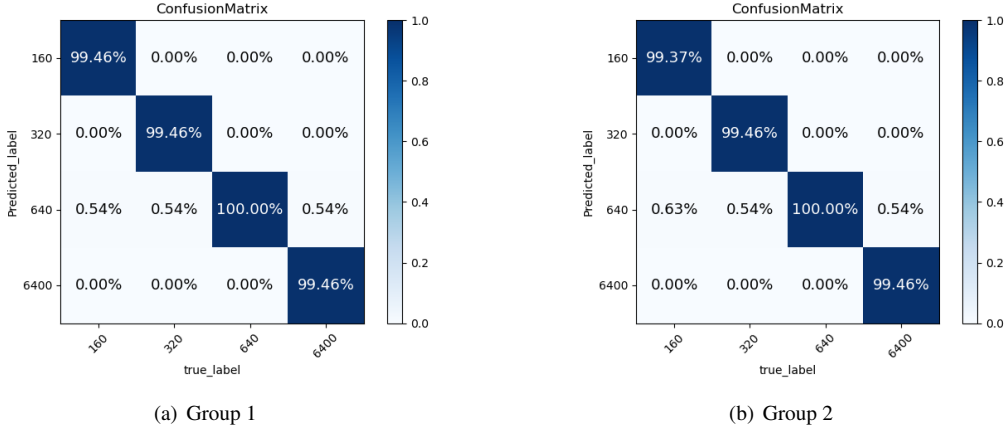


Figure 8: Confusion matrixes in Exp IV.(2).

false detections and missing detections in the visualization result of our method. Compared with several other methods in Fig. 4(a), 4(b) and 4(c), our method obtains the closest visualization result. Our method divides the general structure of shockwave, and the segmentation accuracy reaches 99.76%. The recognition ability of our method in 3D shockwave case is verified.

The above conclusions and visualization results prove that the MLP-based segmentation method proposed in this paper is effective for the flow field segmentation task. Our method is a low-time-consuming and high-accuracy method.

4.3.2. Results for flow field classification

To reduce the impact of random division, each indicator is the average calculation result obtained after repeated training 10 times under different random seeds.

The change curves of accuracy rate and loss value of our method in Exp IV.(1) and Exp IV.(2) are respectively shown in Fig. 5(a) and Fig. 5(b), Fig. 6(a) and Fig. 6(b). In these figures, five sets of experiments fleetly converge to the same value in terms of accuracy and loss, which proves the reproducibility of our method on half-cylinder case.

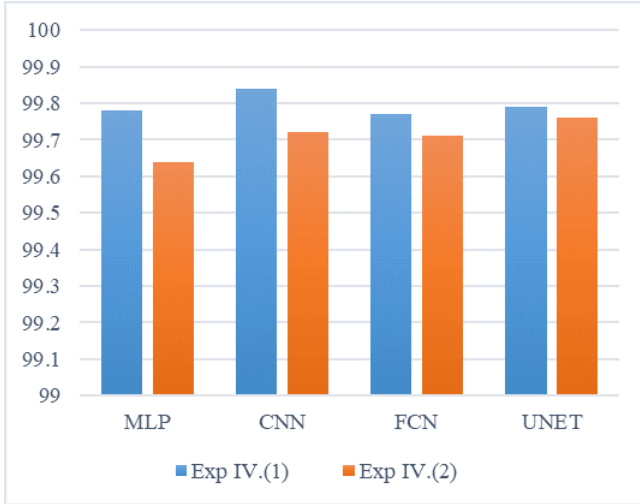
The confusion matrixes of randomly 2 times in 5 times exper-

iments are shown in Fig. 7 and Fig. 8. For classification failure cases, we track the proportion of cases assigned to each error Reynolds number type. The confusion matrix describes the results for all combinations. The diagonal entries of these matrixes show the accuracy with which the network correctly classified the dataset. In the cases of misclassification, off-diagonal entries quantify the degree of confusion between classes.

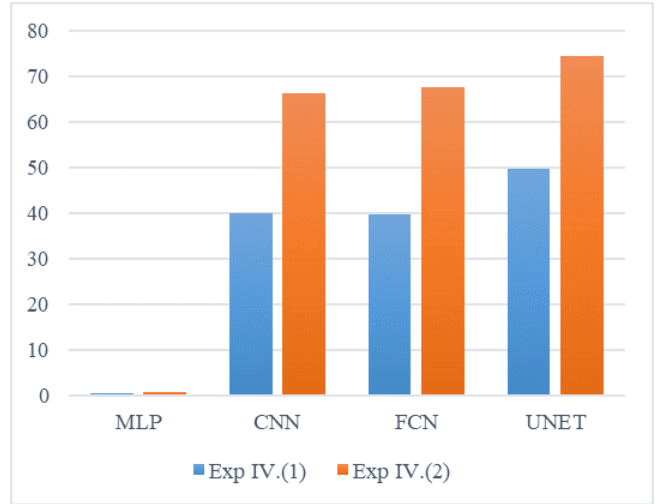
The confusion matrixes in Fig. 7 show that, the prediction accuracy are 99.95% and 100% for the Reynolds number 160 dataset and 99.41% and 99.46% for the Reynolds number 320 dataset in Exp IV.(1). The confusion matrixes in Fig. 8 show that in Exp IV.(2), the prediction accuracy are 99.46% and 99.37% for the Reynolds number 160 dataset, 99.46% and 99.46% for the Reynolds number 320 dataset, 100% and 100% for the Reynolds number 640 dataset, and the prediction accuracy for the dataset with Reynolds number 6400 are both 99.46%. Clearly, in all combinations, the accuracy of predicting the correct class is above 99%, up to 100%.

Fig. 9 shows the intuitive comparison of all methods in Exp IV.(1) and Exp IV.(2) in terms of accuracy rate and training time. The following results can be obtained from Table 4:

- 1) In Exp IV.(1), CNN, FCN and U-Net respectively achieve



(a) accuracy



(b) time consumption

Figure 9: A straight-square comparison plot of experimental results of each classification method in Exp IV.

Table 4

Experiment result for flow field classification

Experiment	Method	Accuracy	Time Consumption(s)
Exp IV.(1)	CNN	99.84%	39.91
	FCN	99.77%	39.72
	U-Net	99.79%	49.76
	MLP	99.78%	0.40
Exp IV.(2)	CNN	99.72%	66.45
	FCN	99.71%	67.54
	U-Net	99.76%	74.64
	MLP	99.64%	0.79

99.84%, 99.77%, and 99.79% accuracy. Our method achieves 99.78% in this experiment, which is 0.06% lower than the best performance (CNN) among baseline methods. In Exp IV.(2), CNN, FCN and U-Net respectively achieve 99.72%, 99.71%, and 99.76% accuracy. Our method achieves 99.64%, which is 0.12% lower than the best performance (U-Net) among baseline methods.

2) In terms of time overhead, CNN, FCN and U-Net respectively cost 39.91 and 66.45 seconds, 39.72 and 67.54 seconds, 49.76 and 74.64 seconds in Exp IV.(1) and Exp IV.(2), which is quite time-consuming. Our method achieves a time consumption of 0.40 and 0.79 seconds, which is 98% less than the best method (FCN, CNN) among baseline methods.

From the above results, we draw the following conclusions:

1) In terms of accuracy, our classification method based on local vorticity changes is slightly inferior to the classification performance of the image-based method. Affected by the sample size of our method, there are 10,240 vorticity change vectors collected in each class in Exp IV.(1) and Exp IV.(2), but the number of image samples collected by the unified dataset is only 1,800 in each class. In this case, our method can still

achieve a classification effect of more than 99%, which proves the rationality of our method.

2) In terms of time consumption, our method discards complex networks in favor of simple linear network for classification. Compared with the popular high-complexity methods (CNN, FCN, UNet), it can greatly simplify the training process and reduce training and verification time.

The above conclusions prove that our classification method proposed in this paper is effective for 3D flow field classification task.

5. Conclusions

The conclusions of our work are as follows:

1) form a robust 3D flow field segmentation method by mapping local velocity information of sample point to the vortex area through deep learning network;

2) construct a novel 3D flow field classification method by establishing the relationship between vorticity, Reynolds number and vortex wake type through deep learning network;

3) compared with Vortex-Net [48], Vortex-Seg-Net [26] and U-Net, the precision of vortex region segmented by our method is significantly improved in some cases while consuming over 50% less time;

4) compared with CNN, FCN and U-Net, the time consumption for flow field classification consumed by our method is reduced by over 98% while keeping the same predicted accuracy.

Our method can be further improved in some aspects. First, we did not conduct research on flow field segmentation in unstructured grids, but only focused on the segmentation of flow fields in structured grids, which limited the application of our method. Besides, our classification method is not extended to turbulent flow, which lacked certain generalization ability. Since the flow field classification method has advantages in the classification of local Reynolds numbers, it can be applied to turbulence identification in the future.

Acknowledgement

The authors also wish to thank Dr. Liwei Hu from University of Electronic Science and Technology of China (UESTC), for discussions on mathematical modelling.

References

- [1] Shi, L., Ma, H., Yu, X., 2020. Pod analysis of the unsteady behavior of blade wake under the influence of laminar separation vortex shedding in a compressor cascade. *Aerospace Science and Technology* 105, 106056.
- [2] Panico, R., Comaron, P., Matuszewski, M., Lanotte, A., Trypogeorgos, D., Gigli, G., Giorgi, M.D., Ardizzone, V., Sanvitto, D., Ballarini, D., 2023. Onset of vortex clustering and inverse energy cascade in dissipative quantum fluids. *Nature Photonics*, 1–6.
- [3] Carbone, M., Bragg, A.D., 2020. Is vortex stretching the main cause of the turbulent energy cascade? *Journal of Fluid Mechanics* 883, R2.
- [4] Pradeep, D., Hussain, F., 2010. Vortex dynamics of turbulence-coherent structure interaction. *Theoretical and Computational Fluid Dynamics* 24, 265–282.
- [5] Yu, A., Qian, Z., Wang, X., Tang, Q., Zhou, D., 2021. Large eddy simulation of ventilated cavitation with an insight on the correlation mechanism between ventilation and vortex evolutions. *Applied Mathematical Modelling* 89, 1055–1073.
- [6] Kenwright, D., Haimes, R., 1997. Vortex identification-applications in aerodynamics: A case study, in: *Proceedings. Visualization'97 (Cat. No. 97CB36155)*, IEEE, pp. 413–416.
- [7] Pierce, B., Moin, P., Sayadi, T., 2013. Application of vortex identification schemes to direct numerical simulation data of a transitional boundary layer. *Physics of Fluids* 25, 015102.
- [8] Jiang, M., Machiraju, R., Thompson, D., 2005. Detection and visualization of vortices. *The visualization handbook* 295.
- [9] Hunt, J., 1987. Vorticity and vortex dynamics in complex turbulent flows. *Transactions of the Canadian Society for Mechanical Engineering* 11, 21–35.
- [10] Liu, C., Wang, Y., Yang, Y., Duan, Z., 2016. New omega vortex identification method. *Science China Physics, Mechanics & Astronomy* 59, 1–9.
- [11] Jeong, J., Hussain, F., 1995. On the identification of a vortex. *Journal of fluid mechanics* 285, 69–94.
- [12] Chong, M.S., Perry, A.E., Cantwell, B.J., 1990. A general classification of three-dimensional flow fields. *Physics of Fluids A: Fluid Dynamics* 2, 765–777.
- [13] Graftieux, L., Michard, M., Grosjean, N., 2001. Combining piv, pod and vortex identification algorithms for the study of unsteady turbulent swirling flows. *Measurement Science and technology* 12, 1422.
- [14] Sadarjoen, I.A., Post, F.H., Ma, B., Banks, D.C., Pagendarm, H.G., 1998. Selective visualization of vortices in hydrodynamic flows, in: *Proceedings Visualization'98 (Cat. No. 98CB36276)*, IEEE, pp. 419–422.
- [15] Serra, M., Haller, G., 2017. Efficient computation of null geodesics with applications to coherent vortex detection. *Proceedings of the Royal Society A: Mathematical, Physical and Engineering Sciences* 473, 20160807.
- [16] Haller, G., Hadjighasem, A., Farazmand, M., Huhn, F., 2016. Defining coherent vortices objectively from the vorticity. *Journal of Fluid Mechanics* 795, 136–173.
- [17] Tian, X., Li, J., 2019. A novel improved fruit fly optimization algorithm for aerodynamic shape design optimization. *Knowledge-Based Systems* 179, 77–91.
- [18] Lin, Q., Hu, J., Zhou, Q., Cheng, Y., Hu, Z., Couckuyt, I., Dhaene, T., 2021. Multi-output gaussian process prediction for computationally expensive problems with multiple levels of fidelity. *Knowledge-Based Systems* 227, 107151.
- [19] Chen, J., Liu, C., Xuan, L., Zhang, Z., Zou, Z., 2022. Knowledge-based turbomachinery design system via a deep neural network and multi-output gaussian process. *Knowledge-Based Systems* 252, 109352.
- [20] Hu, L., Xiang, Y., Zhang, J., Shi, Z., Wang, W., 2022. Aerodynamic data predictions based on multi-task learning. *Applied Soft Computing* 116, 108369.
- [21] Hu, L., Wang, W., Xiang, Y., Zhang, J., 2022a. Flow field reconstructions with gans based on radial basis functions. *IEEE Transactions on Aerospace and Electronic Systems* 58, 3460–3476.
- [22] Epps, B., 2017. Review of vortex identification methods, in: *55th AIAA aerospace sciences meeting*, p. 0989.
- [23] Franz, K., Roscher, R., Milioto, A., Wenzel, S., Kusche, J., 2018. Ocean eddy identification and tracking using neural networks, in: *IGARSS 2018-2018 IEEE International Geoscience and Remote Sensing Symposium, IEEE*, pp. 6887–6890.
- [24] Lguensat, R., Sun, M., Fablet, R., Tandeo, P., Mason, E., Chen, G., 2018. EddyNet: A deep neural network for pixel-wise classification of oceanic eddies, in: *IGARSS 2018-2018 IEEE International Geoscience and Remote Sensing Symposium, IEEE*, pp. 1764–1767.
- [25] Rajendran, V., Kelly, K.Y., Leonardi, E., Menzies, K., 2018. Vortex detection on unsteady cfd simulations using recurrent neural networks, in: *2018 Fluid dynamics conference*, p. 3724.
- [26] Wang, Y., Deng, L., Yang, Z., Zhao, D., Wang, F., 2021. A rapid vortex identification method using fully convolutional segmentation network. *The Visual Computer* 37, 261–273.
- [27] Deng, L., Bao, W., Wang, Y., Yang, Z., Zhao, D., Wang, F., Bi, C., Guo, Y., 2022. Vortex-u-net: An efficient and effective vortex detection approach based on u-net structure. *Applied Soft Computing* 115, 108229.
- [28] Williamson, C.H., Roshko, A., 1988. Vortex formation in the wake of an oscillating cylinder. *Journal of fluids and structures* 2, 355–381.
- [29] Mawat, M.J., 2018. Simulation of cylindrical body structure subjected to flow in different reynolds number regimes. *Muthanna J Eng Technol (MJET)* 6.
- [30] Rashidi, S., Hayatdavoodi, M., Esfahani, J.A., 2016. Vortex shedding suppression and wake control: A review. *Ocean Engineering* 126, 57–80.
- [31] Cann, M., McConkey, R., Lien, F.S., Melek, W., Yee, E., 2021. Mode classification for vortex shedding from an oscillating wind turbine using machine learning, in: *Journal of Physics: Conference Series, IOP Publishing*, p. 012009.
- [32] Wang, M., Hemati, M.S., 2019. Detecting exotic wakes with hydrodynamic sensors. *Theoretical and Computational Fluid Dynamics* 33, 235–254.
- [33] Schnipper, T., Andersen, A., Bohr, T., 2009. Vortex wakes of a flapping foil. *Journal of Fluid Mechanics* 633, 411–423.
- [34] Colvert, B., Alsalmán, M., Kanso, E., 2018. Classifying vortex wakes using neural networks. *Bioinspiration & biomimetics* 13, 025003.
- [35] Alsalmán, M., Colvert, B., Kanso, E., 2018. Training bioinspired sensors to classify flows. *Bioinspiration & biomimetics* 14, 016009.
- [36] Li, B., Zhang, X., Zhang, X., 2020. Classifying wakes produced by self-propelled fish-like swimmers using neural networks. *Theoretical and Applied Mechanics Letters* 10, 149–154.
- [37] Ribeiro, B.L.R., Franck, J.A., 2022. A machine learning approach to classify vortex wakes of energy harvesting oscillating foils. *arXiv preprint arXiv:2205.06367*.
- [38] Wu, J.Z., Ma, H.Y., Zhou, M.D., 2007. *Vorticity and vortex dynamics*. Springer Science & Business Media.
- [39] Liu, C., Gao, Y.s., Dong, X.r., Wang, Y.q., Liu, J.m., Zhang, Y.n., Cai, X.s., Gui, N., 2019. Third generation of vortex identification methods: Omega and liutex/ortex based systems. *Journal of Hydrodynamics* 31, 205–223.
- [40] Chorin, A.J., 1968. Numerical solution of the navier-stokes equations. *Mathematics of computation* 22, 745–762.
- [41] Darwish, M., Moukalled, F., 2016. *The finite volume method in computational fluid dynamics: an advanced introduction with OpenFOAM® and Matlab®*. Springer.
- [42] Han, Z., Zhou, D., Malla, A., Nepali, R., Kushwaha, V., Li, Z., Kwok, K.C., Tu, J., Bao, Y., 2018. Wake-induced vibration interference between a fixed square cylinder and a 2-dof downstream square cylinder at low reynolds numbers. *Ocean Engineering* 164, 698–711.
- [43] Rew, R., Davis, G., 1990. Netcdf: an interface for scientific data access. *IEEE computer graphics and applications* 10, 76–82.
- [44] Perrone, N., Kao, R., 1975. A general finite difference method for arbitrary meshes. *Computers & Structures* 5, 45–57.
- [45] Günther, T., Gross, M., Theisel, H., 2017. Generic objective vortices for flow visualization. *ACM Transactions on Graphics (TOG)* 36, 1–11.
- [46] Popinet, S., 2004. *Free computational fluid dynamics*. ClusterWorld 2, 7.
- [47] Rojo, I.B., Günther, T., 2019. Vector field topology of time-dependent

flows in a steady reference frame. *IEEE Transactions on Visualization and Computer Graphics* 26, 280–290.

- [48] Deng, L., Wang, Y., Liu, Y., Wang, F., Li, S., Liu, J., 2019. A cnn-based vortex identification method. *Journal of Visualization* 22, 65–78.